Investigating Optical Traps: Stiffness Determination and Correlations in Space and Time

Harman Brar[a†]

Dept. of Physics, Simon Fraser University, Burnaby BC

(Dated: April 11, 2023)

[a] lab partner's name: Balhar Mandahar

This technical report presents the results of an optical trapping experiment aimed at studying the correlation between trap strength and laser power, as well as the effects of Brownian motion on the behavior of polystyrene micro-spheres in an aqueous solution. The experiment utilized a diode laser to trap 1–5 µm polystyrene spheres, and their displacement from equilibrium positions was measured over time to determine the strength of the optical trap. As laser power was varied, the trap stiffness measurements exhibited a linear relationship. Additionally, we observed a linear impact of trap strength on the potential energy curves of trapped spheres. Our findings suggest that optical trapping experiments can be used to accurately compare trap strength against laser power while providing insight into micro-particle behavior in aqueous solutions.

I. INTRODUCTION

Optical tweezers, also known as optical traps, were first applied to manipulate micrometer-sized objects in 1986[1]. Arthur Ashkin introduced the use of light to trap matter such as cells, atoms and molecules. By using a focused laser beam's radiation pressure to manipulate and interact with biological particles on sub-nanometer length-scales, optical tweezers have found various applications in the field of physics[2]. A crucial parameter for understanding and optimizing optical trapping experiments is the trap stiffness, which quantifies the strength of the optical trap and how it responds to external forces. Measuring trap stiffness allows researchers to determine the magnitude of forces that can be applied to a trapped particle and can provide insights into the particle's physical properties. This study aims to contribute to the existing knowledge of optical trapping by exploring the understanding of the relationship between trap strength and laser power using variable neutral density filters. We analyze a series of experiments conducted using a custom-built optical trapping setup to methodically vary the laser power and manipulate polystyrene spheres in aqueous solution. We also aim to visualize the probabilistic potential energy of our system and gather an estimate on the optical trap stiffness in multiple directions. Our results provide insights into the relationship between trap strength, laser power and potential energy while contributing to the broader understanding of optical trapping techniques.

II. THEORY

In optical trapping experimentation, small dielectric particles are attracted to regions of high light intensity[2]. A laser beam focused on a particle generates a local intensity maximum, forming a trap. The focused beam of light produces an intensity gradient that exerts a restoring force on the particle at the stable trap position[1]. A Hookean spring implies that a trapped particle experiences the effects of a harmonic potential[3],

$$U(x) = \frac{1}{2}\kappa x^2 \tag{1}$$

This equation is derived by Taylor expanding Hooke's law. The potential energy, $U(x)$ is subject to the force constant κ while x represents the particle's displacement from the center of the trap. The force constant, κ, scales with laser power and can also be referred to as the trap stiffness. This relationship is the same for the y direction, with varying trap strength values. We can use this equation to perform a curve fit of our experimental time series for the potential energy in the x and y directions. Curve fitting allows us to extract important physical parameters such as the trap stiffness and displacement of the trapped particles. By fitting the time series data to the theoretical equation, we can obtain a more accurate estimate of the potential energy and its fluctuations over time. The resulting curve can also be used to quantify the noise level in our measurements and identify any systematic errors in our experimental setup.

Light interacting with the trapped particle can be categorized into two scattering regimes: Mie-scattering and Rayleigh scattering[4]. The Mie-scattering regime occurs when the size of the particle is similar to the wavelength of the incident light. In this regime, the scattered light is strongly dependent on the size of the particle. The Rayleigh regime occurs when the size of the particle is much smaller than the wavelength of the incident light[5]. Here, the scattered light is weakly dependent on the size of the particle. Trapping is most effective at the Mie-scattering regime, when the radius of the bead $R \approx \lambda$, where λ is the laser's wavelength[4]. The trap stiffness is then related to the total beam power by,

$$\kappa \approx U_0\omega \approx \frac{\alpha}{4\pi\omega c}P \tag{2}$$

Here P denotes beam power and c is the speed of light. Using the Mie-scattering limit, $R \approx \omega \approx \lambda$, we input the laser's 658 nm wavelength for the beam waist. The bead dielectric

polarizability α is simplified in the Rayleigh-scattering regime to be,

$$\alpha \approx \frac{n_p^2}{n_0^2} - 1 \tag{3}$$

where n_p and n_0 are the indices of refraction for the polystyrene bead and immersion oil respectively. We are able to use these equations to curve fit our experimental data for different power levels using a neutral density (ND) filter. We can also measure the correlation between the beads position at time 0 and at time t as,

$$\langle x(t)x(0)\rangle = \frac{k_B T}{\kappa} e^{\frac{|t|}{\tau_c}} \tag{4}$$

where the correlation time is given by $\tau_c = \omega_c^{-1} = \gamma/\kappa$. By solving the equation of motion for a trapped bead in a harmonic potential we are able to directly calculate values for various times[6]. The bead positions measured with a significant time interval are non-correlated when $|t| \gg \tau_c$, hence an exponential drop-off is expected to occur[5]. The correlation time τ_c is related to the mechanical properties of the trap, specifically the trap stiffness and the damping coefficient, which is a measure of the drag force that opposes the particle's motion[5]. This result is important in optical trapping as it provides a quantitative measure of the correlation between the position of the trapped bead at different times.

In the case of an optically trapped bead system, the states are represented by the position of the bead within the harmonic potential well defined by Equation (1). Using statistical mechanics, the probability of finding a bead at a particular position can be computed with,

$$p(x) = \frac{1}{Z}\exp\left(\frac{-U(x)}{k_B T}\right) = \frac{1}{Z}\exp\left(\frac{-\kappa x^2}{2k_B T}\right) \tag{5}$$

assuming each dimension is independent. Z is a normalization factor represented by the partition function, while k_B is Boltzmann's constant and T is the temperature of the sample for the experiment. This equation can be used to bin the time series data (in both x and y directions) and plot the potential energy probabilities. The trap strength can also be inferred from another statistical mechanics equation, the equipartition theorem. When an optically trapped particle moves within the harmonic potential well that confines it, the energy of the particle in each dimension can be calculated using Equation (1). Due to the thermal energy being shared equally with each degree of freedom in the system (each degree of freedom has energy $\frac{1}{2}k_B T$), we can equate these to attain

$$\kappa = \frac{k_B T}{\langle x^2 \rangle} \tag{6}$$

The variance of the particle, at a known temperature, is denoted by $\langle x^2 \rangle$[7]. For an optical trap, the equipartition theorem implies that the particle's motion in each spatial dimension is described by a Gaussian distribution with a variance proportional to the temperature and trap stiffness. This is due to the fact that the particle's motion is determined by thermal fluctuations that are modeled as random forces, and the statistics of these forces are Gaussian in nature. Therefore, the equipartition theorem is necessary in optical trapping experiments to understand the expected behavior of trapped particles.

III. METHODS

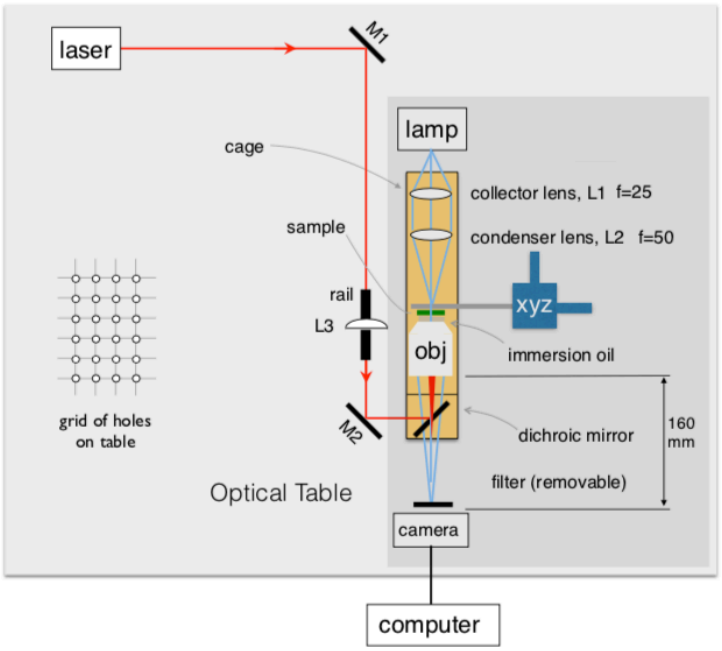

FIG. 1. Simplified schematic showing the optical trapping setup, which uses lenses L1($f = 25$mm) and L2($f = 50$mm) to collect and collimate light, and illuminate the sample with critical illumination. Mirrors M1, M2, and a dichroic mirror steer the laser beam to the objective, which is focused by lens L3. A filter is used to block the laser light during data collection. The setup requires precise alignment with the optical table and rail system.

In the simplified schematic of our optical trap (Figure 1), the setup was composed of a laser, two mirrors (M1 and M2), a dichroic mirror, a focusing lens, and a microscopic objective. The entirety of the setup was constructed on an optical breadboard. The diode laser beam ($\lambda = 658$nm) was directed through the cage system by the mirrors and reflected by the dichroic mirror, which was positioned at a 45° angle. The focusing lens was mounted on a dovetail rail between two apertures and carefully aligned with the laser beam using a cross-carrier mount. The lens was positioned to focus the laser light 160 mm from the back aperture of the objective where a FLIR camera system was mounted and connected to a computer. This created a beam large enough to overfill the back aperture and appear as a uniformly lit red ring around the aperture.

Image capturing was setup on Labview software. The FLIR camera system's gain was set to 10 dB. Increasing the gain amplifies the signal from the camera's sensor, resulting in a brighter image. Conversely, decreasing the gain decreases the amplification of the signal, resulting in a darker image. In addition to the gain, the exposure setting of the camera can be altered to ensure optimal imaging. The exposure controls the amount of time that the camera sensor is exposed to light, and it can be adjusted to prevent overexposure or underexposure of the images. Overexposure can cause saturation of the pixels in the image, which leads to loss of information and reduced accuracy of the measurements. Underexposure can result in a noisy image with poor signal-to-noise ratio. We used an exposure setting of 22 µs to ensure that the images captured were accurate for our analysis. Our FLIR camera was limited to a maximum frame rate of 66 frames per second (FPS)[8]. Consequently, we could have missed some of the high-frequency motion of the bead, which could have affected our analysis. Additionally, the lower frame rate may have resulted in motion blur or decreased temporal resolution of our images, making it more difficult to accurately track the position of the bead and analyze its motion.

The bead test solutions consisted of dilute aqueous 1–5 µm polystyrene spheres. The bead sample was magnetically fixed on the microscope stage with the laser off. The force exerted on the trapped particle is proportional to the gradient of the light intensity, which is strongest at the center of the beam[2]. As a result, the size of the polystyrene microspheres played a crucial role in the trapping process. If the microspheres are too small, they will experience a weak optical force and will be difficult to trap. Conversely, if the microspheres are too large, they may stick together due to van der Waals forces, making them impossible

to trap individually[9]. We found that using 1 µm microspheres was too challenging to trap individually, while larger microspheres were more prone to sticking together. Thus, we opted to use 3 µm microspheres, which were large enough to be individually trapped and small enough to avoid aggregation. This choice of microsphere size helped ensure that our measurements were accurate and reproducible. One droplet of immersion oil was poured in-between the objective and the xyz translation stage. Once the polystyrene spheres were imaged, the laser was turned on, with all viewers wearing laser safety goggles. A short-pass filter was added to the camera to block stray laser light, improving the visibility of the spheres. The focusing lens was adjusted along the rail to align the trap with the microscope's focal plane.

Data collection commenced once a polystyrene sphere was trapped. The bead radius, x-center, and y-center were recorded in pixels for a minimum of sixty seconds. To calibrate our measurements from pixels to physical units, a 0.01 mm calibration slide was placed in the translation stage for one iteration of testing. Further pre-processing steps were taken to ensure data accuracy, including examining the particle time series for drift and outliers, fitting a low-order polynomial to remove background drift, and examining control data from a stuck particle. The trap strength was determined using the equipartition method, Gaussian probability distribution and potential energy curve fitting with Equation (3).

The relationship between trap strength and laser power was examined using a variable neutral density (ND) filter, placed in-between M1 and the laser. To calibrate the filter, the intensity of the unattenuated laser beam was measured and new power readings were taken for various ND filter positions. The trap strength of a single bead was then measured at different laser powers using Equation (4). The obtained force constants (κ_x and κ_y) were plotted against the laser power to further compare against theoretical values.

IV. RESULTS

We initially determined the trap strength in the x and y directions using the equipartition and probability distribution methods listed in Equation (6). The force constants κ_x and κ_y obtained from the equipartition method were 8.12 $\pm$ 0.30 pN/nm and 5.90 $\pm$ 0.18 pN/nm respectively. The variance of the bead was given by the time series data in the x and y directions as seen in Figure 2.

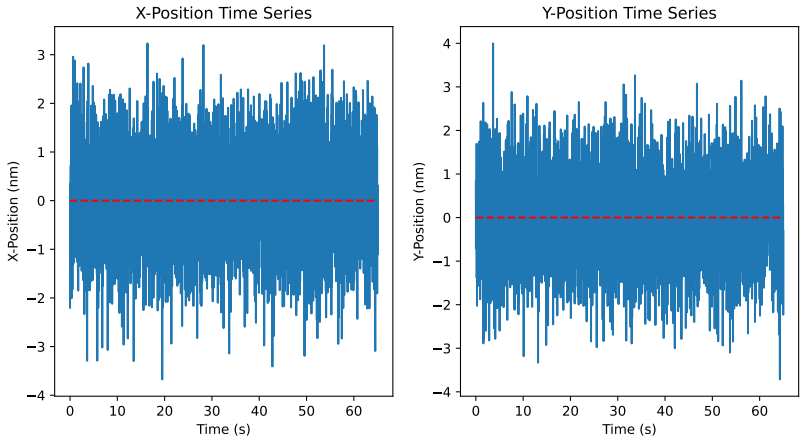

FIG. 2. Time series data of the x and y positions of the bead captured through a Labview tracking software. The frame rate of the FLIR camera was 66 frames per second (FPS).

To conduct our probability distribution measurements, we analyzed the histogram of particle displacement from the trap center by fitting a Gaussian distribution to our time series data. The mean position of the time series was subtracted from the data to remove offsets and reduce the influence of any systematic errors. The standard deviation and mean of particle displacement was used to estimate the stiffness of the trap. The probability distribution method, as seen in Figure 3 yielded a κ_x and κ_y of 8.30 $\pm$ 0.24 pN/nm and 5.14 $\pm$ 0.15 pN/nm. We found these force constants to be in close agreement with our equipartition thereom values.

We further analyzed the dynamics of the trapped particle by calculating the autocorrelation function from Equation (4) for the x and y positions of the bead. As shown in Figure 4, the delta function behaviour of the plots physically show that correlations occur on time scales significantly shorter than the particle's thermal motion. The autocorrelation function was centered about zero, indicating that there was no lag between the two signals[5]. The fluctuations of the autocorrelation function were of order $1/\sqrt{N}$, where N was the number of observations. This result shows that the noise associated with each individual observation becomes less significant as the true underlying signal became more distinct.

The empirical probability distributions were curve fitted to Equation (3) to obtain the potential energy plots in Figure 5. Before curve fitting, the probabilistic potential energy

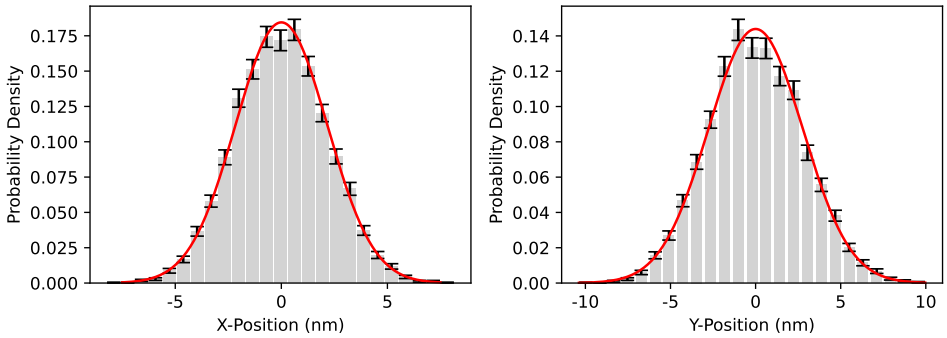

FIG. 3. Histogram of the particle's position in the x and y directions from the Brownian motion time-series data. The plots depict the empirical estimate of probability density. The data was compiled into 20 bins to get an accurate fit. The results were further used in curve fitting of potential energy as seen in Fig. 5. The error bars were calculated by taking the square root of the counts (in each bin) and dividing by the normalization factor, which is the area under the histogram.

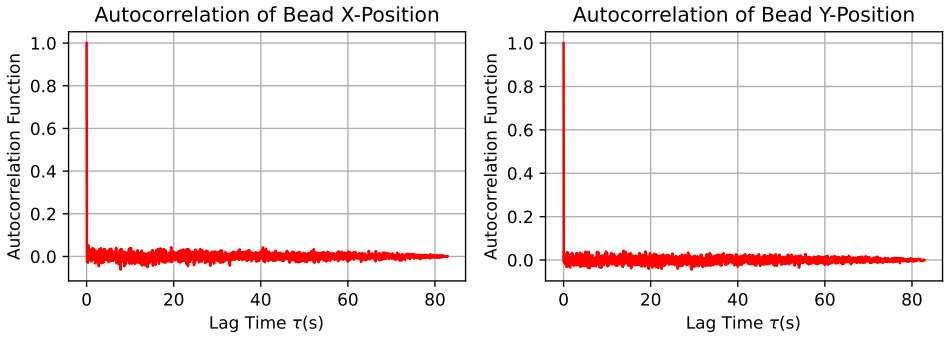

FIG. 4. The normalized auto-correlation functions of the polystyrene bead at it's x and y positions as a function of lag time. The plots show the behaviour of the Brownian time-series data exponentially trending to zero. The auto-correlation function (ACF) measures the correlation between the particle's position at two different time points and depicts positional independence for far-apart times.

points were compiled into 20 bins using Equation (5). The stiffest traps obtained from experimentation were 8.65 $\pm$ 0.26 pN/nm and 5.26 $\pm$ 0.16 pN/nm for κ_x and κ_y. This indicated an acceptable goodness of fit with a χ^2_{red} of 1.50 and 1.11 respectively. From Table I, our results were in close agreement with our equipartition and histogram values.

The measured bead radius range used in experimentation was 2.8 ± 0.2 µm. Due to the

Method	κ_x (pN/nm)	κ_y (pN/nm)
Equipartition Theorem	8.12 ± 0.30	5.90 ± 0.18
Gaussian Distribution	8.30 ± 0.24	5.14 ± 0.15
Potential Energy	8.65 ± 0.26	5.26 ± 0.16
χ^2_{red}	1.11	1.51

TABLE I. Trap strength values for unfiltered laser power. Bead radius range was 2.8 ± 0.2 µm. Last row shows the reduced chi squared values.

effects of bead size on trap stiffness, we averaged our data over five iterations to reduce measurement error. We confirm that as trap stiffness decreased, the potential energy curve became shallower and wider, with a larger equilibrium position. The potential energy curve trends downwards in comparison to the higher trap stiffness plots. This verifies the linear relationship between trap stiffness and potential energy from Equation (3).

To investigate the relationship between trap strength and laser power for various positions of the ND filter, the force constants were plotted against the laser power. The filter was varied from -20mm to 20mm, which resulted in a power reading spectrum from 8.125 mW to 104.7 mW. To calibrate our results and estimate our error, we used a power meter to measured the intensity of the unattenuated laser beam at the position of the filter before and after the microscopic objective. We attained an error measurement of 0.85 mW. As shown in Figure 6, we observed a clear trend of increasing force constants with increasing laser power for both the x and y directions. As evident in our equipartition calculations, κ_y values were smaller than κ_x. This may suggest imperfect alignment with our laser beam entering the microscopic objective. This trend was consistent over the range of laser powers tested, with force constants of 2.23 ± 0.18 pN/nm and 8.97 ± 0.76 pN/nm corresponding to the lowest and highest laser powers, respectively.

V. DISCUSSION

Each experimental method had a distinct set of advantages and disadvantages. The accuracy of the probability distribution method was sensitive to external factors such as vibrations, air currents and slight movements of the experimental setup. It was also necessary to have a sufficiently long time-series to accurately measure the Gaussian probability

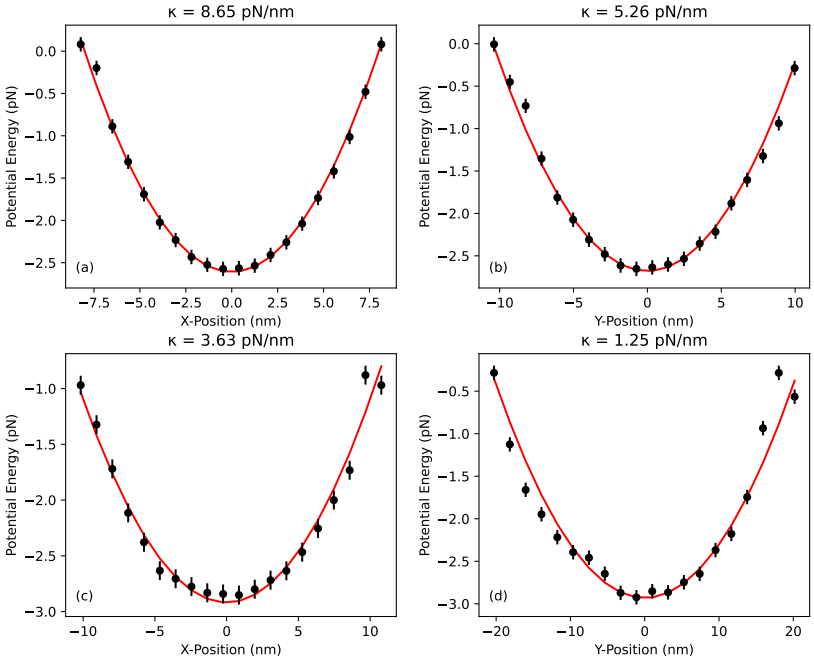

FIG. 5. Plots of the trapped polystyrene bead's potential energy as a function of it's x and y positions. Plots (a) and (b) were taken with an unfiltered laser. Plots (c) and (d) were taken with the ND filter at position -10mm to analyze results for a weaker trap strength. Note the curve's y-axis values are lower in comparison to the unfiltered plots. The parabolic shape of potential energy confirms the behaviour predicted in Equation (1). The error bars were measured by using the time-series of stuck particle as a control, establishing a baseline reference point.

distribution. The longer time-series helped provide a more accurate estimate of the mean and standard deviation while also smoothing out any transient fluctuations in the distribution. In conjunction with the equipartition thereom, the probability distribution gave an acceptable estimate for trap stiffness without necessitating the use of a predefined force. In comparison, the potential energy calculations assume a constant force application over time and negligible influence of external forces on the bead. However, imperfect laser beam alignment and fluctuations in the surrounding medium can cause variations in the force exerted on the bead over time. This method was heavily dependent on the accuracy of the probabilistic binning of the time-series data, hence introducing potential bias. The curve fitting of Equation (1) also assumes a linear relationship between displacement and force.

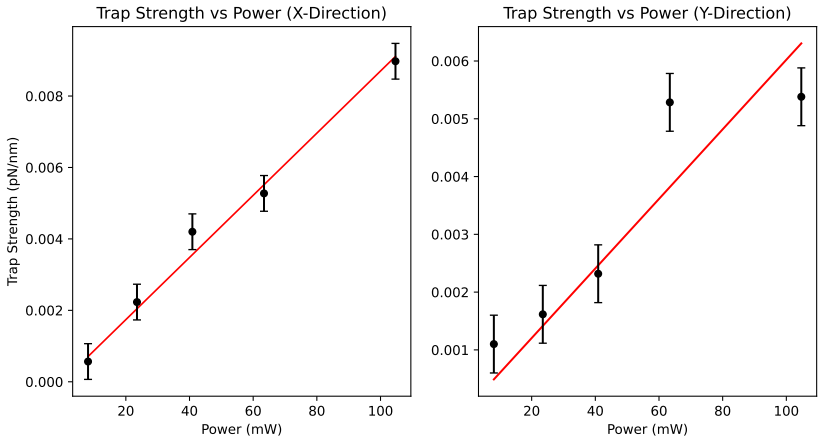

FIG. 6. Plot of the optical trap strength as a function of laser power for x and y directions of the polystyrene sphere. The error bars represent the uncertainty in the trap strength at each laser power and were measured by calibrating our laser power with a power-meter. The linear relationship between the trap strength and laser power verifies expectations from scattering theory.

In reality, this relationship may not be strictly linear and can lead to errors in the determination of trap stiffness. The autocorrelation function was a valuable tool for assessing the thermal motion of the trapped bead, however, it assumes that the statistical properties of the data do not change over time. This may not be true as the trap stiffness can vary due to changes in the laser power, alignment issues or the setup environment. This would affect the accuracy of the analysis. Secondly, the autocorrelation function assumes the motion of the trapped bead is Gaussian, hence following a normal distribution. However, the motion of the trapped particle can be non-Gaussian, such as when the motion is influenced by external factors like hydrodynamic interactions. Acknowledging these limitations, we used a combination of curve fitting procedures and probability distributions to achieve a comprehensive analysis of the experiment.

VI. CONCLUSION

Our investigation of optical trapping demonstrated the effectiveness of our experimental setup in studying the behaviour of trapped polystyrene beads. The histogram and potential energy plots allowed us to investigate the behaviour of the beads in detail while supporting our theoretical derivations for harmonic potentials and trap strength. The linear relationship

between trap stiffness and potential energy was proved experimentally for various values of trap stiffness. For unfiltered laser powers, trap strength values were in good agreement as we measured a low χ^2_{red} value, indicating an acceptable goodness of fit. The autocorrelation followed a delta-function behaviour, indicating a distinct time-series signal. As the laser power was varied using the ND filter, the linear relationship between trap strength was in agreement with theoretical expectations. Together, these analyses offer a comprehensive understanding of the dynamics of the trapped beads and provide a solid foundation for future studies in optical trapping.

VI. REFERENCES

† harman˙brar@sfu.ca

[1] A. Ashkin, J. M. Dziedzic, J. E. Bjorkholm, and Steven Chu, "Observation of a single-beam gradient force optical trap for dielectric particles," *Opt. Lett.* **11**, 288–291 (1986)

[2] A. Ashkin, "Optical trapping and manipulation of neutral particles using lasers", *National Academy of Sciences* **94**(10), 4853-4860 (1997).

[3] T. Tlusty, A. Meller, and R. Bar-Ziv, "Optical gradient forces of strongly localized fields," *Phys. Rev. Lett.* **81**, 1738–1741 (1998).

[4] S. P. Smith, S. R. Bhalotra, A. L. Brody, B. L. Brown, E. K. Boyda, and M. Prenetiss, "Inexpensive optical tweezers for undergraduate laboratories", *Am. J. Phys.* **67**, 26–35 (1999).

[5] J. Bechhoefer and S Wilson. "Faster, cheaper, safer optical tweezers for the undergraduate laboratory", *Am. J. Phys.* **40**(4), (2002).

[6] F, Reif. Fundamentals of Statistical and Thermal Physics, *Waveland Press Inc.* 560-575 (1965).

[7] I. G. Hughes and T. P. A. Hase, "Measurements and their Uncertainties, a Practical Guide to Modern Error Analysis", *Oxford Publishing* (2010).

[8] FLIR Systems. "FLIR Blackfly Camera Instruction Manual" *P/N: BFS-U3-16S2, USB3 Vision* (2018).

[9] A. Kundu, S. Paul, S. Banerjee, and A. Banerjee, "Measurement of Van der Waals force using oscillating optical tweezers", *Appl. Phys. Lett.* **115**, (2019).

We thank K. Winther, D. Lister, V. Sunder and A. Schimmer for valuable assistance at various stages of this work.